bioRxiv preprint doi: https://doi.org/10.1101/702423. this version posted July 15, 2019. The copyright holder for this preprint (which was not certified by peer review) is the author/funder. It is made available under a CC-BY-NC 4.0 International license.

1 # GenEPi: Piezo1-based fluorescent reporter for visualizing
2 # mechanical stimuli with high spatiotemporal resolution

3 **Sine Yaganoglu[1], Nordine Helassa[2,3], Benjamin M. Gaub[1], Maaike Welling[1,4],**
4 **Jian Shi [5], Daniel J. Müller[1], Katalin Török[2], Periklis Pantazis[1,4*]**

5 [1]Department of Biosystems Science and Engineering, Eidgenössische Technische
6 Hochschule (ETH) Zurich, 4058 Basel, Switzerland

7 [2]Molecular and Clinical Sciences Research Institute, St. George's, University of London,
8 UK

9 [3]Department of Cellular and Molecular Physiology, Institute of Translational Medicine,
10 University of Liverpool, UK

11 [4]Department of Bioengineering, Imperial College London, South Kensington Campus,
12 London SW7 2AZ, UK

13 [5]Leeds Institute of Cardiovascular and Metabolic Medicine, LIGHT Laboratories,
14 University of Leeds, Leeds, LS2 9JT, UK

15 *Correspondence to: Periklis Pantazis, p.pantazis@imperial.ac.uk

bioRxiv preprint doi: https://doi.org/10.1101/702423. this version posted July 15, 2019. The copyright holder for this preprint (which was not certified by peer review) is the author/funder. It is made available under a CC-BY-NC 4.0 International license.

16 **Abstract**

17 Mechanosensing is a ubiquitous process to translate external mechanical
18 stimuli into biological responses during development, homeostasis, and disease.
19 However, non-invasive investigation of cellular mechanosensing in complex and
20 intact live tissue remains challenging. Here, we developed GenEPi, a genetically-
21 encoded fluorescent intensiometric reporter for mechanical stimuli based on
22 Piezo1, an essential mechanosensitive ion channel found in vertebrates. We show
23 that GenEPi has high specificity and spatiotemporal resolution for Piezo1-
24 dependent mechanical stimuli, exemplified by resolving repetitive mechanical
25 stimuli of spontaneously contracting cardiomyocytes within microtissues, in a non-
26 invasive manner.

27

bioRxiv preprint doi: https://doi.org/10.1101/702423. this version posted July 15, 2019. The copyright holder for this preprint (which was not certified by peer review) is the author/funder. It is made available under a CC-BY-NC 4.0 International license.

28 **Main Text**

29 Throughout an organism's lifetime, cell mechanosensation (i.e. the ability to
30 perceive and respond to mechanical stimuli in the form of shear stress, tension or
31 compression) is essential in a myriad of developmental, physiological, and
32 pathophysiological processes including embryogenesis, homeostasis, metastasis,
33 and wound healing[1]. How these processes incorporate active feedback via force
34 sensing at the cellular level is an area of active study, and, in recent years, a wide
35 range of tools have been developed to interrogate cell mechanics[2,3].

36 For instance, atomic force microscopy (AFM) and micropipette aspiration
37 have proven to be powerful techniques to quantitatively measure tension in
38 embryos and dissociated cells[4,5]. Other methods, which do not require direct and
39 constant access to the sample, such as droplet-based sensors[6] or optical[7] and
40 magnetic[8] tweezers can modulate probes from a distance and allow precise
41 measurement of molecular to tissue-level forces[2]. Still, these approaches typically
42 require dissociated tissue or their use is complicated by the probe injection and
43 size, which can damage the tissue[2].

44 The necessity to non-invasively measure molecular forces in cells led to the
45 development of genetically-encoded, Förster resonance energy transfer (FRET)-
46 based fluorescent tension sensors, capable of measuring mechanical forces
47 across specific cytoskeletal and adhesion proteins such as vinculin[9], β-spectrin[10]
48 or cadherins[11]. As the specificity and force sensitivity of these probes is defined by
49 the choice of protein and the FRET tension module, their use is restricted to a
50 limited range of biological contexts and force regimes[2,3].

bioRxiv preprint doi: https://doi.org/10.1101/702423. this version posted July 15, 2019. The copyright holder for this preprint (which was not certified by peer review) is the author/funder. It is made available under a CC-BY-NC 4.0 International license.

51 Meanwhile, stretch-activated ion channels, including the Piezo proteins, are
52 capable of responding to various external mechanical stimuli[12,13]. Most vertebrates
53 have two Piezo genes — *Piezo1* and *Piezo2*[12]. While Piezo2 function is mainly
54 restricted to the peripheral nervous system, Piezo1 is expressed in a wide range
55 of tissues and has been shown to contribute to mechanotransduction in various
56 organs[13] (**Supplementary Table 1**). Mutations in human Piezo1 have been
57 implicated in diseases such as dehydrated hereditary stomacytosis[14,15] and
58 general lymphatic dysplasia[16,17]. Global knockout of Piezo1 in mice causes
59 embryonic lethality[18,19], highlighting the importance of this channel for
60 development and homeostasis[13]. How cells and tissues integrate Piezo1 activity
61 has been mainly examined by outputs such as morphological changes, protein
62 expression, electrophysiological signaling, cytosolic calcium (Ca^{2+}) imaging, and
63 transcriptional activity in response to mechanical stimuli[20].

64 In order to develop a non-invasive, genetically-encoded fluorescent reporter
65 for mechanical stimuli that is applicable to a wide variety of cells and types of
66 mechanical stimuli, we set out to generate a reporter of Piezo1 activity. It has been
67 recently shown that the C-terminus of Piezo1 resides within the cytosol and
68 contains the ion-permeating channel[21,22], which has a preference for divalent
69 cations such as Ca^{2+}[21,22]. Upon opening, Ca^{2+} concentration near the channel,
70 referred to as Ca^{2+} microdomain, is typically several fold higher than resting
71 levels[23]. We therefore hypothesized that by targeting a genetically-encoded Ca^{2+}
72 indicator (GECI) to the ion permeating channel of Piezo1, we can obtain an optical
73 readout for its activity.

bioRxiv preprint doi: https://doi.org/10.1101/702423. this version posted July 15, 2019. The copyright holder for this preprint (which was not certified by peer review) is the author/funder. It is made available under a CC-BY-NC 4.0 International license.

74 We reasoned that a fluorescent reporter of channel activation would require
75 a GECI with low Ca^{2+} affinity and a wide dynamic range to reliably monitor the
76 considerable Ca^{2+} increase in the microdomains, while displaying a low response
77 to cytosolic Ca^{2+}, which serves as an important secondary messenger in many
78 other cellular processes[23]. To meet these requirements, we decided to evaluate
79 GCaMPs, a class of GECIs[24], as fluorescent reporters of Piezo1 function. In
80 contrast to FRET-based GECIs, GCaMPs occupy a narrow spectral range,
81 allowing for the simultaneous imaging of multiple fluorescent markers. Progressive
82 protein engineering efforts have yielded GCaMP variants that display a wide
83 dynamic range of response with high signal-to-noise ratios (SNR)[25].
84 In a systematic screen, we generated a library of reporters by fusing five
85 different low-affinity GCaMPs[26,27] (here denoted as GCaMP-G1 - GCaMP-G5)
86 (with K_d-s in the 0.6 to 6 μM range) to the C-terminus of human Piezo1 (**Fig. 1a**).
87 Given the influence of linker length on the sensing mechanism[28], we employed
88 flexible linker peptides with varying lengths to attach GCaMPs to Piezo1
89 (**Supplementary Fig. 1a**). The generated variants were evaluated based on their
90 response to both mechanical stimuli and cytosolic Ca^{2+} fluctuations that were
91 independent of Piezo1 activity. To test their responses to mechanical stimuli,
92 variants were exposed to physiological levels of fluid shear stress[29] (see **Online**
93 **Methods**) (**Supplementary Fig. 1b**), which causes a Piezo1-dependent Ca^{2+}
94 increase in HEK 293T cells[18]. To determine the sensitivity of the variants to
95 intracellular Ca^{2+} levels independent of Piezo1 function, we recorded their
96 response to the Ca^{2+} ionophore ionomycin (**Supplementary Fig. 1b**)[30].

bioRxiv preprint doi: https://doi.org/10.1101/702423. this version posted July 15, 2019. The copyright holder for this preprint (which was not certified by peer review) is the author/funder. It is made available under a CC-BY-NC 4.0 International license.

97 Among the candidates tested, we identified one GCaMP-Piezo1 fusion
98 variant that satisfied our requirements, Piezo1-1xGSGG-GCaMP-G4 (containing
99 the GCaMP6s RS-1 EF-4 variant[27]), hereby referred to as GenEPi (**Fig. 1c**).
100 GenEPi did not affect the viability of HEK 293T cells (**Supplementary Fig. 2**) and
101 its localization in plasma membrane and endoplasmic reticulum reflected that of
102 wild type Piezo1 (**Supplementary note 1** and **Supplementary Fig. 3**). The optical
103 response of GenEPi (**Supplementary Note 1)** to fluid shear stress (**Fig. 1b,c**) was
104 considerably higher (1.61 ±0.09, mean ±s.e.m, n=12 cells) than that of GCaMP6s
105 RS-1 EF-4 (denoted here as GCaMP-G4) expressed in the cytosol (1.36 ±0.02,
106 n=13 cells) (**Fig. 1c**), indicating that channel tethering of GCaMP-G4 in this
107 particular configuration provides optimal access to high Ca^{2+} levels upon Piezo1
108 channel opening in response to mechanical stimuli. Importantly, cytosolic GCaMP-
109 G4 could not distinguish between shear stress and ionomycin and responded to
110 both stimuli (**Fig. 1c**). Furthermore, as GenEPi retained the low affinity for Ca^{2+}
111 (**Supplementary Fig. 4a,b**), it had a low level of response to cytosolic Ca^{2+}
112 induced by ionomycin (1.16 ±0.05, n=15 cells), indistinguishable from the response
113 levels of the control fusion protein, Piezo1-eGFP (1.12 ±0.02, n=19 cells) (**Fig. 1c**).
114 Interestingly, changing the level (1-30 dyn/cm^2) or duration (10-120 sec) of fluid
115 shear stress did not result in any significant difference in GenEPi's response
116 (**Supplementary Fig. 5a,b**), suggesting that the GCaMP response to high Ca^{2+}
117 influx at the channel opening is not concentration-dependent, which confirms
118 previous analysis demonstrating that the GCaMP-G4 response to Ca^{2+} binding is
119 not linear but highly cooperative[27]. The functional specificity of GenEPi was

bioRxiv preprint doi: https://doi.org/10.1101/702423. this version posted July 15, 2019. The copyright holder for this preprint (which was not certified by peer review) is the author/funder. It is made available under a CC-BY-NC 4.0 International license.

120 validated by its selective response to the Piezo1-specific small molecule agonist
121 Yoda1[31], which significantly increased the reporter response (**Fig. 1d**).
122 In addition, we determined GenEPi's response to physiological Ca^{2+}
123 signaling in the cell upon addition of 30 µM ATP. We detected an ATP-dependent
124 cytosolic Ca^{2+} increase using the Ca^{2+} indicator jRCaMP1a (**Fig. 1e**,
125 **Supplementary Fig. 6**)[32] and found that the elevated Ca^{2+} levels were detected
126 by jRCaMP1a, however, not by GenEPi (**Supplementary Fig. 6**). These results
127 indicate that GenEPi is indeed responding specifically to Piezo1-dependent activity
128 and does not sense physiological fluctuations of cytosolic Ca^{2+}, whereas cytosolic
129 Ca^{2+} indicators respond to both Piezo1-dependent and Piezo1–independent
130 stimuli (**Fig.1c, Fig.1e, Supplementary Fig.6**). The specificity of GenEPi's
131 response was further corroborated by the observation that membrane localization
132 of GCaMP-G4 was not sufficient to confer functional specificity (**Supplementary**
133 **Note 2**). Furthermore, channel tethering of all investigated GCaMP variants
134 consistently reduced their response to cytosolic Ca^{2+} evoked by ionomycin
135 (**Supplementary Fig. 1b**), which suggests that genetically-encoded Ca^{2+}
136 indicators placed near the channel are protected from cytosolic Ca^{2+} fluctuations,
137 supporting the microdomain hypothesis[23]. Taken together, GenEPi manifests high
138 SNR and, in contrast to cytosolic Ca^{2+} indicators, demonstrates functional
139 selectivity to the Piezo1-dependent fluid shear stress stimulus.
140 As Piezo1 is known to respond to other forms of mechanical stimuli, such
141 as compression, we characterized the force sensitivity and temporal kinetics of
142 GenEPi under this stimulus. We turned to a previously described AFM-based

bioRxiv preprint doi: https://doi.org/10.1101/702423. this version posted July 15, 2019. The copyright holder for this preprint (which was not certified by peer review) is the author/funder. It is made available under a CC-BY-NC 4.0 International license.

143 setup[33] that allows probing Piezo1 sensitivity to mechanical stimuli while
144 simultaneously recording the optical response of GenEPi (**Fig. 2a,b**). We applied
145 precisely-timed compressive forces ranging from 100 nN to 400 nN with 50 nN
146 increments on single HEK 293T cells expressing GenEPi using a 5 µm bead
147 attached to an AFM cantilever (**Fig. 2c**). These compressive forces related to
148 pressures ranging from 2.6 to 10.2 kPa or 19.1 to 76.5 mmHg (**Supplementary**
149 **Note 3**). GenEPi responded to short (250 ms) compressive forces with fast
150 kinetics, but on average with comparable signal amplitude to shear stress (1.65
151 ±0.12, n=21 cells) (**Fig. 2d**). While GenEPi signals in response to compressive
152 forces were abolished in response to GsMTx-4, an inhibitor of Piezo1[34] (**Fig. 2e**),
153 the Piezo1-eGFP fusion did not show any optical response (**Fig. 2d**). The precise
154 control of stimulation level and duration in this experimental setup allowed us to
155 characterize the force sensitivity and duration of Piezo1-induced fluorescent
156 signals reported by GenEPi and cytosolic GCaMP-G4. Although HEK 293T cells
157 express small amounts of Piezo1, channel overexpression is required to reliably
158 confer mechanical sensitivity to HEK 293T cells[35] (**Supplementary Fig. 7**). To
159 compare Piezo1-induced fluorescent signals, we applied timed compression onto
160 GenEPi transfected cells and control cells co-transfected with human Piezo1 and
161 cytosolic GCaMP-G4. Measured threshold forces were comparable for GenEPi
162 and cytosolic GCaMP4 (243.50 ±13.68 nN and 241.20 ±13.87 nN, each n=21 cells,
163 respectively) (**Fig. 2f**), demonstrating that the mechanical sensitivity of the channel
164 is not affected by the protein fusion. Similarly, electrochemical response, ion
165 selectivity and channel kinetics of Piezo1 within GenEPi were preserved in

bioRxiv preprint doi: https://doi.org/10.1101/702423. this version posted July 15, 2019. The copyright holder for this preprint (which was not certified by peer review) is the author/funder. It is made available under a CC-BY-NC 4.0 International license.

166 response to mechanical stimulation, the agonist Yoda1, and the generic inhibitor
167 ruthenium red (**Supplementary Fig. 8-10**).

168 GenEPi's response to cantilever-triggered compression lasted on average
169 7.56 ±1.09 seconds (n=16 cells), which was much shorter than that of the cytosolic
170 indicator (18.39 ±1.84 seconds, n=27 cells) (**Fig. 2g**), while the electrochemical
171 inactivation kinetic of GenEPi in response to mechanical stimuli was comparable
172 to Piezo1 and shorter than that of the Piezo1 delayed inactivation mutant
173 R2456H[36] (**Supplementary Fig. 11**). In conclusion, GenEPi provides not only high
174 spatial resolution and functional specificity, when compared to cytosolic Ca^{2+}
175 indicators, but also offers a gain in temporal resolution in response to mechanical
176 stimuli.

177 In order to test GenEPi's functional specificity and performance in a three-
178 dimensional and multicellular environment, we tested its response to homeostatic
179 cell motions, such as cardiomyocyte contraction. To this end, we generated
180 doxycycline-inducible GenEPi mouse embryonic stem cells (mESCs)[37]
181 (**Supplementary Fig. 12a**) and differentiated these cells to cardiomyocytes[38]. We
182 confirmed GenEPi's activity in undifferentiated mESC by monitoring its specific
183 response to Yoda1 (**Supplementary Fig. 12b**). After 10 days of differentiation
184 (**Supplementary Fig. 13a)**, spontaneously beating patches of cells could be
185 identified in microtissues (**Supplementary Video 1)** consisting predominantly of
186 cardiomyocytes (**Supplementary Fig. 13d)**, and other mesodermal lineage cells,
187 such as smooth muscle cells and endothelial cells (**Supplementary Fig. 13c,e**).
188 Within some beating patches, we observed cells that displayed noticeable GenEPi

bioRxiv preprint doi: https://doi.org/10.1101/702423. this version posted July 15, 2019. The copyright holder for this preprint (which was not certified by peer review) is the author/funder. It is made available under a CC-BY-NC 4.0 International license.

189 responses to the cardiomyocyte contraction-triggered mechanical stimulation. The
190 response amplitude range (F/F_0=1.15 to 2.29) was comparable to that of shear
191 stress and compressive forces, yet the responses lasted less than a second (**Fig.**
192 **3a-c and Supplementary Video 2**). The subcellular and subsecond GenEPi
193 response (**Fig. 3a-c**) rate was qualitatively coupled to the autonomous beating of
194 the cardiomyocytes but at a slower frequency (**Supplementary Video 2**), which
195 could be also observed in the electrochemical response of Piezo1 within GenEPi
196 in response to repetitive mechanical stimulation (**Supplementary Fig. 14**).

197 In order to confirm our observation that the source of these GenEPi
198 responses were indeed cardiomyocyte contractions, we applied blebbistatin, a
199 myosin inhibitor, which blocks the contractions and uncouples mechanical stimuli-
200 induced Ca^{2+} influx from Ca^{2+} processes accompanying spontaneous cell
201 contractions[39]. Fast GenEPi responses (**Fig. 3d**) decreased when contractions
202 stopped in response to blebbistatin (**Fig. 3e**), as demonstrated by the significant
203 decrease in the amplitude and frequency of the GenEPi response (**Fig. 3f-h**),
204 confirming the cardiomyocyte contractions as the source of GenEPi signals.
205 Hence, GenEPi shows a high spatiotemporal resolution of Piezo1 activity in
206 microtissues, capable of specifically sensing repetitive and spontaneous
207 mechanical stimuli of beating cardiomyocytes.

208 In summary, we introduced GenEPi as an intensiometric, genetically-
209 encoded reporter for mechanical stimuli. GenEPi provides a specific and non-
210 invasive functional readout of Piezo1 activity in response to mechanical stimuli,
211 including shear stress and compressive forces with high spatiotemporal resolution

bioRxiv preprint doi: https://doi.org/10.1101/702423. this version posted July 15, 2019. The copyright holder for this preprint (which was not certified by peer review) is the author/funder. It is made available under a CC-BY-NC 4.0 International license.

212 in cells as well as small microtissues. This was achieved by successfully targeting
213 a low-affinity GCaMP to the Ca^{2+} microdomain near the Piezo1 channel, which
214 resulted in specificity for only Piezo1-dependent Ca^{2+} signals. Due to the highly
215 cooperative Ca^{2+} sensing mechanism of GCaMP, GenEPi does not quantitatively
216 report mechanical stimuli; however, GenEPi has a significantly broader
217 applicability as compared to other genetically-encoded mechanical reporters,
218 since Piezo1 has been identified to play a central role for mechanosensation in an
219 increasing number of cell types and contexts (**Supplementary Table 1**). For
220 instance, Piezo1 has been shown to sense mechanical properties of the
221 environment of neural progenitor cells, influencing neuronal differentiation[40], and
222 to play a role in regulating volume of red blood cells[41], where changes in shear
223 stress and other mechanical forces are common. While the use of GenEPi requires
224 overexpression of the Piezo1 channel; the role of GenEPi in various contexts can
225 be studied using the inducible GenEPi mESC line, with full control over the
226 expression levels of Piezo1, using doxycycline. Altogether, these features render
227 GenEPi an ideal tool to elucidate the full extent to which mechanical signals, and
228 more specifically Piezo1 channels, regulate development, physiology, and
229 disease.

230 **ACKNOWLEDGEMENTS**

231 We thank members of the Pantazis group, especially A.Y. Sonay for
232 discussion and feedback. We thank W.P. Dempsey for help in designing the sketch
233 depicting the mechanism of the reporter and feedback on the manuscript. This
234 work was supported by the Swiss National Science Foundation (SNF grant no.

bioRxiv preprint doi: https://doi.org/10.1101/702423. this version posted July 15, 2019. The copyright holder for this preprint (which was not certified by peer review) is the author/funder. It is made available under a CC-BY-NC 4.0 International license.

235 31003A_144048 to P.P.), the European Union Seventh Framework Program
236 (Marie Curie Career Integration Grant (CIG) no. 334552 to P.P.), the Royal Society
237 Wolfson Research Merit Award holder to P.P., the Rubicon grant from the
238 Netherlands Organisation for Scientific Research and a fellowship from the Peter
239 und Traudl Engelhorn Stiftung to M.W., the European Molecular Biology
240 Organization (EMBO; ALTF 424-2016 to B.M.G.), the NCCR Molecular Systems
241 Engineering, the Wellcome Trust Project Grant 094385/Z/10/Z and BBSRC Project
242 Grant (BB/M02556X/1 to K.T.) and British Heart Foundation Intermediate Basic
243 Science Research Fellowship (FS/17/56/32925 to N.H. and FS/17/2/32559 to
244 J.S.). The Institute of Translational Medicine, Cellular and Molecular Physiology,
245 University of Liverpool is thanked for the use of Zeiss LSM 800 confocal
246 microscope.

247 **AUTHOR CONTRIBUTIONS**

248 S.Y. conceived and S.Y. and P.P. refined the idea. S.Y. designed, carried
249 out, and analyzed all experiments with the exception of the following: K.T.
250 designed the four GCaMPs (G1-G4), N.H. carried out *in situ* affinity
251 measurements; B.M.G. and D.J.M. designed and carried out AFM-based force
252 spectroscopy and simultaneous confocal microscopy; M.W. generated the dox-
253 inducible mESC line and carried out differentiation experiments; J.S. carried out
254 patch-clamp electrophysiology. S.Y. and P.P. wrote the manuscript and all authors
255 contributed to editing the manuscript. P.P. supervised the project.

256 **DATA AVAILABILITY STATEMENT**

bioRxiv preprint doi: https://doi.org/10.1101/702423. this version posted July 15, 2019. The copyright holder for this preprint (which was not certified by peer review) is the author/funder. It is made available under a CC-BY-NC 4.0 International license.

257 The data that support the findings of this study are available from the
258 corresponding author upon request.

259 **REFERENCES**
260

261 1 Heisenberg, C. P. & Bellaiche, Y. Forces in tissue morphogenesis and
262 patterning. *Cell* **153**, 948-962, doi:10.1016/j.cell.2013.05.008 (2013).
263 2 Campas, O. A toolbox to explore the mechanics of living embryonic tissues.
264 *Seminars in cell & developmental biology* **55**, 119-130,
265 doi:10.1016/j.semcdb.2016.03.011 (2016).
266 3 Freikamp, A., Cost, A. L. & Grashoff, C. The Piconewton Force Awakens:
267 Quantifying Mechanics in Cells. *Trends in cell biology* **26**, 838-847,
268 doi:10.1016/j.tcb.2016.07.005 (2016).
269 4 Maitre, J. L., Niwayama, R., Turlier, H., Nedelec, F. & Hiiragi, T. Pulsatile cell-
270 autonomous contractility drives compaction in the mouse embryo. *Nature*
271 *cell biology* **17**, 849-855, doi:10.1038/ncb3185 (2015).
272 5 Krieg, M. *et al.* Tensile forces govern germ-layer organization in zebrafish.
273 *Nature cell biology* **10**, 429-436, doi:10.1038/ncb1705 (2008).
274 6 Campas, O. *et al.* Quantifying cell-generated mechanical forces within living
275 embryonic tissues. *Nature methods* **11**, 183-189, doi:10.1038/nmeth.2761
276 (2014).
277 7 Bambardekar, K., Clement, R., Blanc, O., Chardes, C. & Lenne, P. F. Direct laser
278 manipulation reveals the mechanics of cell contacts in vivo. *Proceedings of*
279 *the National Academy of Sciences of the United States of America* **112**, 1416-
280 1421, doi:10.1073/pnas.1418732112 (2015).
281 8 Savin, T. *et al.* On the growth and form of the gut. *Nature* **476**, 57-62,
282 doi:10.1038/nature10277 (2011).
283 9 Grashoff, C. *et al.* Measuring mechanical tension across vinculin reveals
284 regulation of focal adhesion dynamics. *Nature* **466**, 263-266,
285 doi:10.1038/nature09198 (2010).
286 10 Krieg, M., Dunn, A. R. & Goodman, M. B. Mechanical control of the sense of
287 touch by beta-spectrin. *Nature cell biology* **16**, 224-233,
288 doi:10.1038/ncb2915 (2014).
289 11 Borghi, N. *et al.* E-cadherin is under constitutive actomyosin-generated
290 tension that is increased at cell-cell contacts upon externally applied stretch.
291 *Proceedings of the National Academy of Sciences of the United States of*
292 *America* **109**, 12568-12573, doi:10.1073/pnas.1204390109 (2012).
293 12 Coste, B. *et al.* Piezo1 and Piezo2 are essential components of distinct
294 mechanically activated cation channels. *Science (New York, N.Y.)* **330**, 55-60,
295 doi:10.1126/science.1193270 (2010).
296 13 Wu, J., Lewis, A. H. & Grandl, J. Touch, Tension, and Transduction - The
297 Function and Regulation of Piezo Ion Channels. *Trends in biochemical sciences*
298 **42**, 57-71, doi:10.1016/j.tibs.2016.09.004 (2017).

bioRxiv preprint doi: https://doi.org/10.1101/702423. this version posted July 15, 2019. The copyright holder for this preprint (which was not certified by peer review) is the author/funder. It is made available under a CC-BY-NC 4.0 International license.

299 14 Andolfo, I. *et al.* Multiple clinical forms of dehydrated hereditary
300 stomatocytosis arise from mutations in PIEZO1. *Blood* **121**, 3925-3935,
301 s3921-3912, doi:10.1182/blood-2013-02-482489 (2013).
302 15 Albuisson, J. *et al.* Dehydrated hereditary stomatocytosis linked to gain-of-
303 function mutations in mechanically activated PIEZO1 ion channels. *Nature*
304 *communications* **4**, 1884, doi:10.1038/ncomms2899 (2013).
305 16 Fotiou, E. *et al.* Novel mutations in PIEZO1 cause an autosomal recessive
306 generalized lymphatic dysplasia with non-immune hydrops fetalis. *Nature*
307 *communications* **6**, 8085, doi:10.1038/ncomms9085 (2015).
308 17 Lukacs, V. *et al.* Impaired PIEZO1 function in patients with a novel autosomal
309 recessive congenital lymphatic dysplasia. *Nature communications* **6**, 8329,
310 doi:10.1038/ncomms9329 (2015).
311 18 Li, J. *et al.* Piezo1 integration of vascular architecture with physiological force.
312 *Nature* **515**, 279-282, doi:10.1038/nature13701 (2014).
313 19 Ranade, S. S. *et al.* Piezo1, a mechanically activated ion channel, is required
314 for vascular development in mice. *Proceedings of the National Academy of*
315 *Sciences of the United States of America* **111**, 10347-10352,
316 doi:10.1073/pnas.1409233111 (2014).
317 20 Gottlieb, P. A. A Tour de Force: The Discovery, Properties, and Function of
318 Piezo Channels. *Current topics in membranes* **79**, 1-36,
319 doi:10.1016/bs.ctm.2016.11.007 (2017).
320 21 Coste, B. *et al.* Piezo proteins are pore-forming subunits of mechanically
321 activated channels. *Nature* **483**, 176-181, doi:10.1038/nature10812 (2012).
322 22 Gottlieb, P. A., Bae, C. & Sachs, F. Gating the mechanical channel Piezo1: a
323 comparison between whole-cell and patch recording. *Channels (Austin, Tex.)*
324 **6**, 282-289, doi:10.4161/chan.21064 (2012).
325 23 Clapham, D. E. Calcium signaling. *Cell* **131**, 1047-1058,
326 doi:10.1016/j.cell.2007.11.028 (2007).
327 24 Nakai, J., Ohkura, M. & Imoto, K. A high signal-to-noise Ca(2+) probe
328 composed of a single green fluorescent protein. *Nature biotechnology* **19**,
329 137-141, doi:10.1038/84397 (2001).
330 25 Chen, T. W. *et al.* Ultrasensitive fluorescent proteins for imaging neuronal
331 activity. *Nature* **499**, 295-300, doi:10.1038/nature12354 (2013).
332 26 Sun, X. R. *et al.* Fast GCaMPs for improved tracking of neuronal activity.
333 *Nature communications* **4**, 2170, doi:10.1038/ncomms3170 (2013).
334 27 Helassa, N., Podor, B., Fine, A. & Torok, K. Design and mechanistic insight into
335 ultrafast calcium indicators for monitoring intracellular calcium dynamics.
336 *Scientific reports* **6**, 38276, doi:10.1038/srep38276 (2016).
337 28 Chen, X., Zaro, J. L. & Shen, W. C. Fusion protein linkers: property, design and
338 functionality. *Advanced drug delivery reviews* **65**, 1357-1369,
339 doi:10.1016/j.addr.2012.09.039 (2013).
340 29 Malek, A. M., Alper, S. L. & Izumo, S. Hemodynamic shear stress and its role in
341 atherosclerosis. *Jama* **282**, 2035-2042 (1999).
342 30 Zhivotovsky, B. & Orrenius, S. Calcium and cell death mechanisms: a
343 perspective from the cell death community. *Cell calcium* **50**, 211-221,
344 doi:10.1016/j.ceca.2011.03.003 (2011).

bioRxiv preprint doi: https://doi.org/10.1101/702423. this version posted July 15, 2019. The copyright holder for this preprint (which was not certified by peer review) is the author/funder. It is made available under a CC-BY-NC 4.0 International license.

345 31 Syeda, R. *et al.* Chemical activation of the mechanotransduction channel
346 Piezo1. *eLife* **4**, doi:10.7554/eLife.07369 (2015).
347 32 Dana, H. *et al.* Sensitive red protein calcium indicators for imaging neural
348 activity. *eLife* **5**, doi:10.7554/eLife.12727 (2016).
349 33 Gaub, B. M. & Muller, D. J. Mechanical Stimulation of Piezo1 Receptors
350 Depends on Extracellular Matrix Proteins and Directionality of Force. *Nano*
351 *letters* **17**, 2064-2072, doi:10.1021/acs.nanolett.7b00177 (2017).
352 34 Bae, C., Sachs, F. & Gottlieb, P. A. The mechanosensitive ion channel Piezo1 is
353 inhibited by the peptide GsMTx4. *Biochemistry* **50**, 6295-6300,
354 doi:10.1021/bi200770q (2011).
355 35 Sachs, F. Mechanical transduction by ion channels: A cautionary tale. *World*
356 *journal of neurology* **5**, 74-87, doi:10.5316/wjn.v5.i3.74 (2015).
357 36 Zarychanski, R. *et al.* Mutations in the mechanotransduction protein PIEZO1
358 are associated with hereditary xerocytosis. *Blood* **120**, 1908-1915,
359 doi:10.1182/blood-2012-04-422253 (2012).
360 37 Iacovino, M. *et al.* Inducible cassette exchange: a rapid and efficient system
361 enabling conditional gene expression in embryonic stem and primary cells.
362 *Stem cells (Dayton, Ohio)* **29**, 1580-1588 (2011).
363 38 Wang, H., Hao, J. & Hong, C. C. Cardiac induction of embryonic stem cells by a
364 small molecule inhibitor of Wnt/beta-catenin signaling. *ACS chemical biology*
365 **6**, 192-197, doi:10.1021/cb100323z (2011).
366 39 Farman, G. P. *et al.* Blebbistatin: use as inhibitor of muscle contraction.
367 *Pflugers Archiv : European journal of physiology* **455**, 995-1005,
368 doi:10.1007/s00424-007-0375-3 (2008).
369 40 Pathak, M. M. *et al.* Stretch-activated ion channel Piezo1 directs lineage
370 choice in human neural stem cells. *Proceedings of the National Academy of*
371 *Sciences of the United States of America* **111**, 16148-16153,
372 doi:10.1073/pnas.1409802111 (2014).
373 41 Faucherre, A., Kissa, K., Nargeot, J., Mangoni, M. E. & Jopling, C. Piezo1 plays a
374 role in erythrocyte volume homeostasis. *Haematologica* **99**, 70-75,
375 doi:10.3324/haematol.2013.086090 (2014).
376
377

bioRxiv preprint doi: https://doi.org/10.1101/702423. this version posted July 15, 2019. The copyright holder for this preprint (which was not certified by peer review) is the author/funder. It is made available under a CC-BY-NC 4.0 International license.

378 **FIGURE LEGENDS**

379 **Figure 1. *In vitro* characterization of GenEPi shows that the reporter has**
380 **functional specificity.** (**a**) GenEPi sensing mechanism. GCaMP is targeted near
381 the C-terminal Piezo1 channel. When mechanical stimuli induce channel opening,
382 incoming Ca^{2+} (in yellow) binds to GCaMP, causing an increase in green
383 fluorescence. (**b**) Representative example of GenEPi activation and F/F_0 signal
384 intensity profile (black) in response to 10 dyn/cm^2 shear stress (blue) in HEK 293T
385 cells. Time stamps in the images correspond to the stimulation and response
386 profile in the graph. Scale bar, 10 µm. (**c**) Response of HEK 293T cells expressing
387 Piezo1 and GCaMP-G4 (n=13, shear stress; n=18, ionomycin), GenEPi (n=12,
388 shear stress; n=15, ionomycin), or Piezo1-eGFP (n=16, shear stress, n=19,
389 ionomycin) to shear stress and ionomycin. Two-tailed Mann-Whitney test,
390 ****=p<0.0001; *=p<0.05; n.s.=p>0.05, data from three independent experiments.
391 (**d**) Response of GenEPi expressing HEK 293T cells to 10 µM Yoda1 (n=14) or
392 DMSO (n=17). Two-tailed Mann-Whitney test, ****= p<0.0001, data from three
393 independent experiments. (**e**) Response of GenEPi and jRCaMP1a expressing
394 HEK 293T cells (dots, n=19) to intracellular Ca^{2+} triggered by 30 µM ATP. Welch's
395 t-test, ****= p<0.0001, data from six independent experiments. (**c, e**) Grey bars are
396 means ±s.e.m.

397 **Figure 2. GenEPi retains force sensitivity and shows fast temporal resolution**
398 **in response to compression.** (**a**) Representative images of AFM cantilever
399 stimulation of GenEPi expressing HEK 293T cells stimulated by the compressing
400 AFM cantilever. Brightfield image of cantilever position before and during

bioRxiv preprint doi: https://doi.org/10.1101/702423. this version posted July 15, 2019. The copyright holder for this preprint (which was not certified by peer review) is the author/funder. It is made available under a CC-BY-NC 4.0 International license.

401 stimulation and (**b**) fluorescent image of the stimulated cell before and after
402 stimulation. Scale bar, 10 µm. (**c**) The mechanical stimulation procedure, of
403 compressive forces ranging from 129-370 nN (purple) along with the brightfield
404 (grey) and fluorescent (black) traces from the cell depicted in **a,b**. (**d**) Amplitude of
405 Ca^{2+} responses from GenEPi (n=21), and Piezo-eGFP (n=45) expressing cells.
406 Two-tailed Mann-Whitney test, ****= p<0.0001. (**e**) Amplitude of Ca^{2+} responses
407 from GenEPi expressing cells before (n=13) and after addition of 3 µM GsMTx-4
408 (n=11). Two-tailed Mann-Whitney test, ****= p<0.0001. (**f**) Threshold forces and
409 pressures for cells co-transfected with human Piezo1 and cytosolic GCaMP-G4
410 (n=21), n.s.=p>0.05, Unpaired t-test. (**g**) Duration of Ca^{2+} responses from cells co-
411 transfected with cytosolic GCaMP-G4 and human Piezo1 (n=27) and GenEPi
412 (n=16). Two-tailed Mann-Whitney test, ****= p<0.0001. Grey bars are means
413 ±s.e.m., data from three independent experiments.

414 **Figure 3. GenEPi reports cardiomyocyte contraction-triggered mechanical**
415 **stimulation with high spatiotemporal resolution.** (**a**) Intensity profile of a single
416 cell attached to the beating patch expressing GenEPi in response to the
417 autonomous beating of the cardiomyocytes. (**b**) Magnified intensity profile from the
418 boxed region in red in (**a**) of GenEPi's responses (red arrowhead) and
419 fluorescence artifacts (grey arrowhead) upon cardiomyocyte contraction. (**c**)
420 Time-lapse images of GenEPi response depicted in (**b**). Scale bar, 5 µm. (**d**)
421 Representative F/F_0 signal from a ROI in a cell in response to cardiomyocyte
422 contraction. (**e**) Same ROI as in (**d**), after addition of 100 µM blebbistatin. (**f**) Total
423 area, (**g**) frequency of peaks, and (**h**) maximum F/F_0 measurement for each ROI

bioRxiv preprint doi: https://doi.org/10.1101/702423. this version posted July 15, 2019. The copyright holder for this preprint (which was not certified by peer review) is the author/funder. It is made available under a CC-BY-NC 4.0 International license.

424 before, and after the addition of blebbistatin. n=15 ROIs, error bar=s.e.m. Wilcoxon
425 rank-sum test, *= p<0.05, **= p<0.01. Grey bars are means ±s.e.m., data from
426 three independent experiments.

427 **ONLINE METHODS**

428 **Molecular cloning**

429 We obtained the human Piezo1 cDNA from Kazusa Inc, Japan. Generation
430 of the first four types of GCaMPs; mGCaMP6s-EF4 (GCaMP-G1), mGCaMP6f-
431 EF4 (GCaMP-G2), mGCaMP6s RS1-EF3 (GCaMP-G3) and mGCaMP6s RS1-
432 EF4 (GCaMP-G4), were described elsewhere[1]. Fast-GCaMP-EF20 (here denoted
433 as GCaMP-G5) was a gift from Samuel Wang (Addgene plasmid #52645)[2]. pGP-
434 CMV-NES-jRCaMP1a was a gift from Douglas Kim (Addgene plasmid #61462)[3].

435 Piezo1 was amplified using Herculase II fusion DNA Polymerase (600675,
436 Agilent Technologies) and all Ca^{2+} indicators with various linker lengths were
437 amplified with Phusion high-fidelity DNA polymerase (M0530S, NEB). List of
438 primers, ordered from Sigma-Aldrich, can be found in **Supplementary Table 2**.
439 Piezo1 and the Ca^{2+} indicators were introduced using restriction cloning and T4
440 DNA ligase (NEB). The Lck targeting sequence flanking restriction sites were
441 synthesized by Genewiz, and introduced upstream of GCaMP-G4 and GCaMP-
442 G5. All restriction enzymes were purchased from NEB. PCR and digestion
443 products were purified using QIAquick PCR purification kit (28104, Qiagen) and
444 QIAquick Gel Extraction kit (28704, Qiagen). Ligations were carried out using T4
445 Ligase (NEB) at 24°C for 1 hour followed by chemical transformation using Turbo
446 ultracompetent *E.coli* based on K12 strain (NEB) and grown on Agar LB plates

bioRxiv preprint doi: https://doi.org/10.1101/702423. this version posted July 15, 2019. The copyright holder for this preprint (which was not certified by peer review) is the author/funder. It is made available under a CC-BY-NC 4.0 International license.

447 (Q60120 and Q61020, Thermo Fisher) and LB liquid media (244610, BD
448 Bioscience) supplemented with appropriate antibiotics (100 µg ml^{-1} Ampicillin or
449 50 µg ml^{-1} Kanamycin, Sigma-Aldrich). Clones were screened using restriction
450 digest and sequenced by Microsynth. Plasmid DNA isolation was carried out using
451 ZR Plasmid Miniprep (D4054, Zymo Research).

452 **Cell culture and transfection**

453 HEK 293T cells were obtained from ATCC (ATCC CRL-3216). Cells were
454 cultured at 37°C, 5% CO_2, in high glucose DMEM with GlutaMAX (10569010,
455 Thermo Fisher), supplemented with 10% FBS (P40-37500, Pan Biotech) and
456 1X Penicillin-Streptomycin solution (15140122, Thermo Fisher). Cells were
457 routinely tested and were negative for mycoplasma infection using Mycoplasma
458 detection kit (B39032, LuBioScience GmBH). Plasmid DNA for transfection was
459 isolated from 50 ml LB culture (244610, BD Bioscience) containing appropriate
460 antibiotics using the Zymopure Plasmid Midiprep kit (D4200, Zymo Research). The
461 amount of DNA was measured using the Nanodrop 2000c Spectrophotometer
462 (Thermo Fisher) and 400-800 ng of each plasmid was introduced into cells using
463 nucleofection (V4XC-2024, Lonza). Briefly, 70-80% confluent cells were washed
464 with 1X Dulbecco's Phosphate Buffered Saline (DPBS) (D8537-500ML, Sigma-
465 Aldrich) and dissociated using 0.05% Trypsin-EDTA (25300054, Thermo Fisher).
466 10 µl of the cell suspension was mixed with 10 µl Trypan Blue (0.4%) (15250061,
467 Thermo Fisher) and added to the cell counting slide (1450011, Bio Rad
468 Laboratories AG). Cell count and cell viability were automatically calculated by the
469 TC10 Cell Counter (Bio Rad Laboratories AG) and only cell suspensions with

bioRxiv preprint doi: https://doi.org/10.1101/702423. this version posted July 15, 2019. The copyright holder for this preprint (which was not certified by peer review) is the author/funder. It is made available under a CC-BY-NC 4.0 International license.

470 >90% viability were used for transfections. For fluid shear stress and chemical
471 treatment experiments, 10^6 cells were centrifuged for 5 minutes at 90xg and
472 resuspended in 100 µl of SF cell line nucleofector solution. The cells mixed with
473 400-800 ng of each plasmid were then transferred into the nucleofection cuvette
474 and pulsed using the program CM-150 (V4XC-2024, Lonza). 500 µl of fresh media
475 was added to the cells, which were then transferred to a well in a 6-well plate
476 (140675, Thermo Fisher). At 24 hours post transfection, the cells were dissociated
477 and counted as previously described. The cells were then seeded onto ibitreat flow
478 chambers (Ibidi u-slide-VI 0.4, 80606, Ibidi GmbH) for fluid shear stress
479 experiments or ibitreat coated 8-well slides (80826, Ibidi GmbH) with a density of
480 75,000 cells per channel or well.

481 For experiments to test the response of the reporter to various chemicals,
482 we used 1 µM ionomycin (I3909-1ML, Sigma-Aldrich), 30 µM ATP (A6559-
483 25UMO, Sigma Aldrich) diluted in DPBS, 10 µM Yoda1 (5586, Tocris Bioscience)
484 diluted in DMSO (D8418, Sigma Aldrich) or 2.5 µM GsMTx-4 (Pepta Nova GmBH)
485 diluted in water.

486 For AFM experiments, HEK 293T cells were transfected using lipofection.
487 Briefly, 1.5 10^6 cells were seeded in a T25 flask (CLS430639, Sigma-Aldrich) the
488 day before transfection. 4 µg of the reporter, or 1.6 µg of GCaMP-G4 and 3.6 µg
489 of Piezo1 were diluted in 250 µl of Opti-MEM (31985062, Thermo Fisher), while
490 20 µl of Lipofectamine 2000 reagent (11668019, Thermo Fisher) was also diluted
491 in 250 µl of Opti-MEM. After 5 minutes of incubation, the two solutions were mixed
492 together and further incubated for 20 minutes. The solution was then introduced to

bioRxiv preprint doi: https://doi.org/10.1101/702423. this version posted July 15, 2019. The copyright holder for this preprint (which was not certified by peer review) is the author/funder. It is made available under a CC-BY-NC 4.0 International license.

493 cells and washed away with fresh medium after 4 hours. At 24 hours post
494 transfection, the cells were dissociated and counted as previously described, and
495 seeded onto 35 mm-wide cover-glass bottom Fluorodishes (FD35-100, World
496 Precision Instruments), with a density of 300,000 cells per plate.

497 For the *in situ* affinity measurements, HeLa cells were cultured in DMEM
498 containing non-essential amino-acids (Life Technologies), penicillin/streptomycin
499 (100 U ml^{-1}, 100 μg ml^{-1}, respectively) and 10% heat inactivated FBS (Life
500 Technologies) at 37 °C in an atmosphere of 5% CO_2. Cells were plated on 35 mm
501 glass bottom culture dishes (MatTek) and allowed 24 hours to adhere before
502 transfection with FuGENE HD (Promega) following the manufacturer's
503 instructions. Cells were maintained for 12-24 hours before being used in
504 experiments.

505 **Generation of inducible GenEPi-mESC cell line (iGenEPi)**

506 Doxycycline-inducible GenEPi-mESCs were generated using ZX1 mESCs
507 carrying rtTA in the Rosa26 locus and dox-inducible cre flanked by self-
508 incompatible LoxP sites in the HPRT locus[4], kindly provided by Dr. Michael Kyba.
509 ZX1 mESCs were cultured in DMEM (Life Technologies), 15% FBS (PAN Biotech),
510 2 mM L-Glutamine (Invitrogen), 1X non-essential amino acids, 0.1 mM β-
511 mercaptoethanol, 100 U ml^{-1} leukemia inhibitory factor (Peprotech), 1 μM
512 PD0325901 (Selleckchem) and 3 μM CHIR99201 (R&D Systems) on gelatin
513 coated plates. Prior to electroporation, ZX1 mESCs were exposed to 500 nl ml^{-1}
514 doxycycline for 24 hours. 1 x 10^6 ZX1 mESCs were electroporated with 3 μg p2lox
515 plasmid in which GenEPi was cloned between LoxP sites in a 0.4 cm

bioRxiv preprint doi: https://doi.org/10.1101/702423. this version posted July 15, 2019. The copyright holder for this preprint (which was not certified by peer review) is the author/funder. It is made available under a CC-BY-NC 4.0 International license.

516 electroporation cuvette at 230 mV, 500 µF and maximum resistance in a Biorad
517 electroporator (Biorad Genepulser Xcell). 24 hours after electroporation, antibiotic
518 selection was started with 300 µg/mL G418 (Sigma). Colonies that incorporated
519 GenEPi were verified by FACS analysis and expanded. Dox-inducible GenEPi
520 mESCs were differentiated to cardiomyocytes as previously described[5]. GenEPi
521 mESCs were seeded as 500 cell / 20 µl in hanging drops on non-adherent plates
522 to generate embryoid bodies (EBs) in EB medium, IMDM (Life Technologies), 20%
523 FBS (PAN Biotech), 2 mM L-Glutamine (Invitrogen), 1X non-essential amino acids
524 and 0.1 mM β-mercaptoethanol. After 2 days, EBs were transferred to uncoated
525 petridishes. From day 3-5, 1 µM XAV939 was added to the culture conditions and
526 EBs were plated on gelatin coated dished from day 4. Beating EBs appeared at
527 day 10 of differentiation. Beating EBs were manually dissected and dissociated
528 using 2 mg/ml Collagenase/Dispase (Sigma) to generate smaller beating patches
529 and single cells (Supplementary Fig. 10). For blebbistatin experiments, 40-120 µM
530 Blebbistatin (B0560, Sigma Aldrich) diluted in DMSO (D8418, Sigma Aldrich) was
531 applied to the cells in 20 µM steps until contractions were stopped.

532 **Determination of cell viability and cell toxicity**

533 Cell viability was determined using trypan blue exclusion assay. Briefly, cells in
534 triplicates seeded in 6-well tissue culture plates (Thermo Fisher) were transfected
535 with varying concentrations of GenEPi or GCaMP-G4 and human Piezo1. At 24
536 and 48 hours post transfection, cells were washed with 1X PBS twice and
537 detached using 0.05% Trypsin-EDTA (25300054, Thermo Fisher). 10 µl of cell
538 suspension was then mixed with 10 µl 0.4% Trypan Blue, and 10 µl of this mixture

bioRxiv preprint doi: https://doi.org/10.1101/702423. this version posted July 15, 2019. The copyright holder for this preprint (which was not certified by peer review) is the author/funder. It is made available under a CC-BY-NC 4.0 International license.

539 was added to the cell counting slide (C10228, Thermo Fisher) and measured using
540 Countess II Automated cell counter (Thermo Fisher). The viability was expressed
541 as a fold difference of the untreated samples for each time point.

542 To determine cell toxicity, lactate dehydrogenase (LDH) assay (Life
543 Technologies) was used on GenEPi or GCaMP-G4 and human Piezo1 transfected
544 cells according to manufacturer's instructions. Briefly, GenEPi or GCaMP-G4 and
545 human Piezo1 transfected cells in triplicates were seeded in 96-well tissue culture
546 plates (167008, Thermo Fisher). After 48 hours, 10 µl of Cell Lysis buffer was
547 added to a non-transfected cell triplicate and incubated for 45 minutes at 37°C,
548 5% CO_2 to obtain maximum LDH activity. Afterwards 50 µl of each cell sample as
549 well as the non-transfected cells for spontaneous LDH activity and maximum LDH
550 activity was transferred into a new 96-well plate and mixed with 50 µl reaction
551 mixture. Following 30 minutes of incubation at room temperature, 50 µl stop
552 solution was added and the absorbance was measured at 490 nm and 680 nm
553 using Tecan M1000 plate reader. To determine LDH activity, the absorbance
554 values for 680 nm were subtracted from that of 490 nm. Percentage of cytotoxicity
555 based on maximum LDH activity was determined as following: 100 x (cell sample
556 LDH activity-spontaneous LDH activity)/(maximum LDH activity-spontaneous LDH
557 activity).

558 **Fluid shear stress applications**

559 We used the ibidi pump system (#10905, Ibidi GmBH). Fluid shear stress
560 levels were calibrated and imaging solution viscosity of the perfusion solution was
561 determined according to manufacturer's instructions. Depending on the level of

bioRxiv preprint doi: https://doi.org/10.1101/702423. this version posted July 15, 2019. The copyright holder for this preprint (which was not certified by peer review) is the author/funder. It is made available under a CC-BY-NC 4.0 International license.

562 fluid shear stress applied, perfusion set yellow-green (#10964, for 5-30 dyn/cm^2)
563 or perfusion set white (#10963, for 1-5 dyn/cm^2) were used. Representative fluid
564 shear stress application traces are shown in **Fig. 1c**.

565 **Confocal microscopy**

566 Images were acquired using the Zeiss 780 NLO Confocor 3 equipped with
567 an argon laser for 458 and 488 nm excitation, a diode pumped solid-state laser for
568 561 nm excitation and a HeNe laser for 633 nm excitation. Images of single cells
569 were acquired using the C Apo 40x/1.1 W DICIII objective, excited with 488 nm for
570 reporter, and 561 nm for tdTomato and jRCaMP1a excitation, respectively. In order
571 to ensure fast image acquisition, we imaged single cells in a small region of interest
572 within the field of view, recording a single z-plane over several minutes. Live
573 imaging of cells was carried out in Live Cell Imaging Solution (A14291DJ,
574 ThermoFisher).

575 **Atomic force microscopy (AFM)-based force spectroscopy and**
576 **simultaneous confocal microscopy**

577 Prior to the experiment, 5 µm diameter silica beads (Kisker Biotech) were
578 glued to the free end of tipless cantilevers (CSC-37, Micromash HQ) using UV glue
579 (Dymax) and cured under UV light for 20 minutes. Cantilevers with beads were
580 plasma treated for 5 minutes using a plasma cleaner (Harrick Plasma) to ensure a
581 clean surface, and subsequently mounted on a standard glass cantilever holder
582 (JPK Instruments) of the AFM. Cells cultured on glass-bottom Petri dishes were
583 kept at 37ºC using a Petri dish heater (JPK Instruments). For the mechanical
584 stimulation, an AFM (CellHesion 200, JPK Instruments) was mounted on an

bioRxiv preprint doi: https://doi.org/10.1101/702423. this version posted July 15, 2019. The copyright holder for this preprint (which was not certified by peer review) is the author/funder. It is made available under a CC-BY-NC 4.0 International license.

585 inverted confocal microscope (Observer Z1, LSM 700, Zeiss). Cantilevers were
586 calibrated using the thermal noise method[6]. Mechanical stimulation protocols were
587 programmed using the JPK CellHesion software. During the mechanical stimulus,
588 the AFM lowered the bead on the cantilever onto the cell with a speed of 10 μm s^{-1}
589 until reaching the preset force, kept the preset force constant for
590 250 milliseconds, and then retracted with a speed of 100 μm s^{-1}. Preset forces
591 were applied in intervals from 100 nN to 400 nN with 50 nN increments with the
592 time between intervals ranging from 10–25 seconds. Representative mechanical
593 stimulation traces are shown in **Fig 2c**.
594 Confocal imaging was performed using an inverted laser-scanning
595 microscope (LSM 700, Zeiss) equipped with a 25x/0.8 LCI PlanApo water
596 immersion objective (Zeiss). Time-lapse images were acquired with 100–
597 300 milliseconds time resolution and acquisition was initiated > 10 seconds before
598 the onset of the mechanical stimulus. Time-lapse images of Ca^{2+} responses were
599 analyzed using the built-in ZEN blue software.
600 **Patch-clamp electrophysiology**
601 Human embryonic kidney 293T (HEK293T) cells were transfected with the
602 plasmids using lipofectamine 2000 (Invitrogen). 48 hours after transfection, whole-
603 cell and cell-attached patch-clamp recordings were made with the Axopatch-200B
604 (Axon Instruments, Inc.) equipped with the Digidata 1550B and the pCLAMP 10.6
605 software (Molecular Devices, Sunnyvale, CA, USA) on the cells at room
606 temperature. The tip resistance of recording glass pipettes was between 3 and
607 5 MΩ. The currents were sampled at 20 kHz and filtered at 2 kHz. The mechanical

bioRxiv preprint doi: https://doi.org/10.1101/702423. this version posted July 15, 2019. The copyright holder for this preprint (which was not certified by peer review) is the author/funder. It is made available under a CC-BY-NC 4.0 International license.

608 force was applied through a recording pipette using a Patchmaster-controlled
609 pressure-clamp HSPC-1 device (ALA Scientific Instruments).

610 For whole-cell recordings, the external solution consisted of (in mM) 133
611 NaCl, 3 KCl, 2.5 $CaCl_2$, 1 $MgCl_2$, 10 HEPES and 10 glucose (pH 7.3 with NaOH).
612 The pipette solution was composed of (in mM) 133 CsCl, 1 $CaCl_2$, 1 $MgCl_2$, 5
613 EGTA, 10 HEPES, 4 MgATP and 0.4 Na_2GTP (pH 7.3 with CsOH).

614 For cell-attached recordings, the extracellular solutions were composed of
615 (in mM) 140 KCl, 1 $MgCl_2$, 10 glucose and 10 HEPES (pH 7.3 with KOH). The
616 pipette solutions consisted of (in mM) 130mM NaCl, 5 KCl, 1 $CaCl_2$, 1 $MgCl_2$, 10
617 TEA-Cl and 10 HEPES (pH 7.3 with NaOH).

618 ***In situ* Ca^{2+} titration of GenEPi**

619 GenEPi-transfected HeLa cells were permeabilized using 150 µM β-escin
620 (in 20 mM Na^+-HEPES, 140 mM KCl, 10 mM NaCl, 1 mM $MgCl_2$, pH 7.2) for
621 4 minutes. The solution was replaced with "zero free Ca^{2+}" solution (20 mM Na^+-
622 HEPES, 140 mM KCl, 10 mM NaCl, 1 mM $MgCl_2$, 10 mM EGTA, pH 7.2) and
623 various Ca^{2+} concentrations (0.001, 0.01, 0.1, 1, 10, 50, 500, 10000 µM free Ca^{2+})
624 were applied in the presence of 10 µM ionomycin and 4 µM thapsigargin. Free
625 Ca^{2+} concentrations were calculated using the two-chelators Maxchelator
626 program[7].

627 Cells were examined with a Zeiss LSM 800 confocal microscope equipped
628 with a 63x/1.4 Plan-Apochromat oil immersion objective and a 488 nm diode laser
629 as excitation light source. Emitted light was collected through Variable Secondary
630 Dichroics (VSDs) onto a GaAsP-PMT detector. The fluorescence signal was

bioRxiv preprint doi: https://doi.org/10.1101/702423. this version posted July 15, 2019. The copyright holder for this preprint (which was not certified by peer review) is the author/funder. It is made available under a CC-BY-NC 4.0 International license.

631 monitored over an elliptical region of interest (ROI) in the plasma membrane using
632 the ImageJ program. Data obtained from 12 to 42 cells (from at least three
633 independent experiments) was plotted and analysed on GraphPad Prism 6. The
634 fluorescence dynamic range $(F_{max}\text{-}F_0)/F_0$ or $\Delta F/F_0$ was expressed as mean ± s.e.m.
635 The Ca^{2+} dissociation constant (K_d) and cooperativity (n) were obtained by fitting
636 the data to the Hill equation.

637 **Live staining and immunochemistry**

638 Live cell staining of cells was achieved using the Image-IT LIVE plasma
639 membrane and nuclear labeling kit cell staining kit (I34406, Thermo-Fisher), and
640 the ER tracker red (E34250, Thermo-Fisher) according to product specifications.
641 For antibody stainings, cells were fixed in 4% paraformaldehyde (15714-S,
642 Lucerna Chem AG) for 5 minutes, washed with PBS and blocked using Max Block
643 blocking medium (15252, Active Motif) supplemented with 0.1% TritonX-100
644 (T8787, Sigma Aldrich). Cells were then incubated with anti-GFP antibody
645 (ab6673, Abcam) or anti-Piezo1 antibody (ab82336, Abcam) diluted in Max Block
646 blocking medium. After several washing steps with PBS, the cells were incubated
647 with goat anti-rabbit Alexa Fluor-633 (A-21071) or donkey anti-goat Alexa Fluor-
648 633 (A-21082, Thermo Fisher) as well as DAPI (62248, Thermo Fisher). Mouse
649 embryos and mESCs were fixed in 10% paraformaldehyde (15714-S, Lucerna
650 Chem AG) for 10 minutes, permeabilized with PBS supplemented with
651 0.1% TritonX-100 (T8787, Sigma Aldrich) and blocked with 10% Donkey Serum
652 (17-000-121, Jackson ImmunoResearch) in PBS supplemented with
653 0.1% TritonX-100. Samples were then incubated with anti-GFP antibody (ab6673,

bioRxiv preprint doi: https://doi.org/10.1101/702423. this version posted July 15, 2019. The copyright holder for this preprint (which was not certified by peer review) is the author/funder. It is made available under a CC-BY-NC 4.0 International license.

654 Abcam), anti-mouse E-cadherin (AF748-SP, Techne AG), anti-cardiac Troponin T
655 antibody (ab8295, Abcam), anti-smooth muscle myosin heavy chain II antibody
656 (ab53219, Abcam) or anti-CD31/PECAM-1 antibody (AF3628, R&D systems)
657 diluted in 10% Donkey Serum (17-000-121, Jackson ImmunoResearch) in PBS
658 supplemented with 0.1% TritonX-100. After several washing steps with PBS, the
659 samples were incubated with donkey anti-goat Alexa Fluor-594 (A-11058, Thermo
660 Fisher), goat anti-mouse Alexa Fluor-568 (A-11004), goat anti-rabbit Alexa Fluor-
661 633 (A-21071) or donkey anti-goat Alexa Fluor-633 (A-21082, Thermo Fisher) as
662 well as DAPI (62248, Thermo Fisher).

663 **Image processing and analysis**

664 For the shear stress experiments, and time-lapse upon experiments with
665 application of a chemical, the cells were automatically segmented using a MATLAB
666 script. Briefly, the signals from the cytosolic tdTomato or jRCaMP1a were
667 automatically identified, and high intensity pixels were used to generate a mask.
668 This mask was then applied to the time series images of the reporter and the
669 cytosolic signal and single cell intensities were extracted for each time point. This
670 information allowed us to get the traces for the intensiometric reporter response of
671 each cell. Ca^{2+} responses were expressed as fluorescence levels normalized to
672 baseline (F/F_0). To obtain (F/F_0), we divided the fluorescence levels (F) by the
673 baseline fluorescence of the cell (fluorescence of the first five frames, F_0).

674 During the AFM experiments, mechanical stimulation of cells with the
675 cantilever caused cytosolic or membrane bound fluorophores to move in or out of
676 the confocal imaging plane, creating fluorescence artifacts. These artifacts were

bioRxiv preprint doi: https://doi.org/10.1101/702423. this version posted July 15, 2019. The copyright holder for this preprint (which was not certified by peer review) is the author/funder. It is made available under a CC-BY-NC 4.0 International license.

677 clearly distinguishable from Piezo1 receptor mediated Ca^{2+} influx, since (i) they
678 showed strong symmetry with stepwise increase and decrease of fluorescence (ii)
679 were very short in duration, and (iii) appeared synchronously with the mechanical
680 stimulus and were thus preceding the Ca^{2+} responses. **Fig. 2c** illustrates such an
681 example of fluorescence artifacts and Ca^{2+} responses. Any fluorescent signal that
682 was greater than the artifact was classified as "response", anything below was
683 defined as noise. The resulting signal trace was processed as described above.
684 The duration of the signal was calculated by subtracting the first time point
685 fluorescence signal is higher than artifact from the time point signal goes back to
686 the baseline. Baseline was calculated as average fluorescence of 5 seconds
687 preceding the stimulus.

688 **Statistical analysis**

689 All data are expressed means ±s.e.m. Sample sizes (n) are provided in the
690 text or figure legend of each experiment. Each experiment has been repeated
691 independently at least 3 times. Each data set was subjected to Shapiro-Wilk
692 normality test to determine whether the data set has a Gaussian distribution;
693 $p>0.05$ indicated it has a Gaussian distribution, and $p<0.05$ indicated it did not.
694 When all of the compared data sets had Gaussian distribution, two-tailed Student's
695 t-test was applied to compare two independent datasets; with an *F*-test to compare
696 variances. When F-test resulted in $p<0.05$, Welch's correction was applied to the
697 t-test. When more than 2 datasets were present with Gaussian distribution, one-
698 way ANOVA was used to compare datasets, followed by Holm-Sidak's *post hoc*
699 multiple comparisons test. When at least one of the compared data sets did not

bioRxiv preprint doi: https://doi.org/10.1101/702423. this version posted July 15, 2019. The copyright holder for this preprint (which was not certified by peer review) is the author/funder. It is made available under a CC-BY-NC 4.0 International license.

700 have a Gaussian distribution, Mann-Whitney test was applied to compare two
701 independent datasets; and Wilcoxon rank-sum test was applied when the data sets
702 were paired. When more than 2 datasets were present without Gaussian
703 distribution, Kruskal-Wallis test was applied, followed by Dunn's *post hoc* multiple
704 comparisons test. For all statistics, p-value were reported, with n.s.=p>0.05,
705 *=p<0.05, **=p<0.01, ***=p<0.001 and ****=p<0.0001.

706 **REFERENCES FOR ONLINE METHODS**

707 1 Helassa, N., Podor, B., Fine, A. & Torok, K. Design and mechanistic insight into
708 ultrafast calcium indicators for monitoring intracellular calcium dynamics.
709 *Scientific reports* **6**, 38276, doi:10.1038/srep38276 (2016).
710 2 Sun, X. R. *et al.* Fast GCaMPs for improved tracking of neuronal activity.
711 *Nature communications* **4**, 2170, doi:10.1038/ncomms3170 (2013).
712 3 Dana, H. *et al.* Sensitive red protein calcium indicators for imaging neural
713 activity. *eLife* **5**, doi:10.7554/eLife.12727 (2016).
714 4 Iacovino, M. *et al.* Inducible cassette exchange: a rapid and efficient system
715 enabling conditional gene expression in embryonic stem and primary cells.
716 *Stem cells (Dayton, Ohio)* **29**, 1580-1588 (2011).
717 5 Wang, H., Hao, J. & Hong, C. C. Cardiac induction of embryonic stem cells by a
718 small molecule inhibitor of Wnt/beta-catenin signaling. *ACS chemical biology*
719 **6**, 192-197, doi:10.1021/cb100323z (2011).
720 6 Hutter, J. L. & Bechhoefer, J. Calibration of atomic‐force microscope tips.
721 *Review of Scientific Instruments* **64**, 1868-1873, doi:10.1063/1.1143970
722 (1993).
723 7 Schoenmakers, T. J., Visser, G. J., Flik, G. & Theuvenet, A. P. CHELATOR: an
724 improved method for computing metal ion concentrations in physiological
725 solutions. *BioTechniques* **12**, 870-874, 876-879 (1992).
726

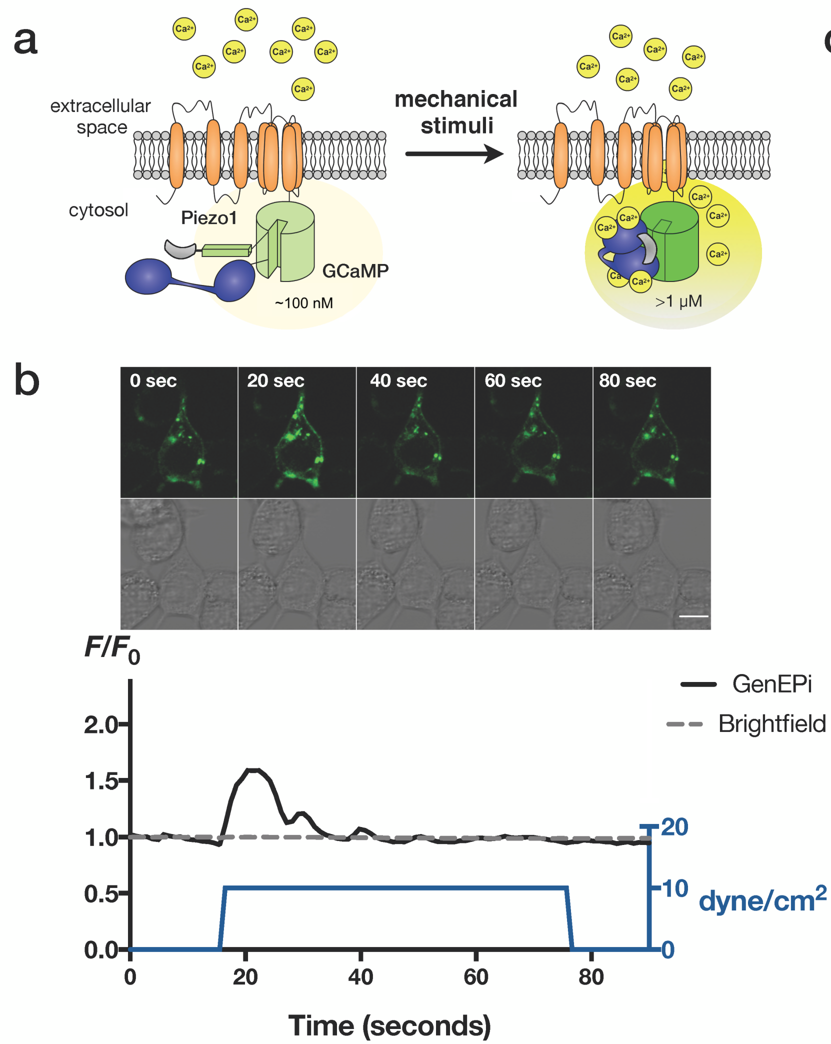

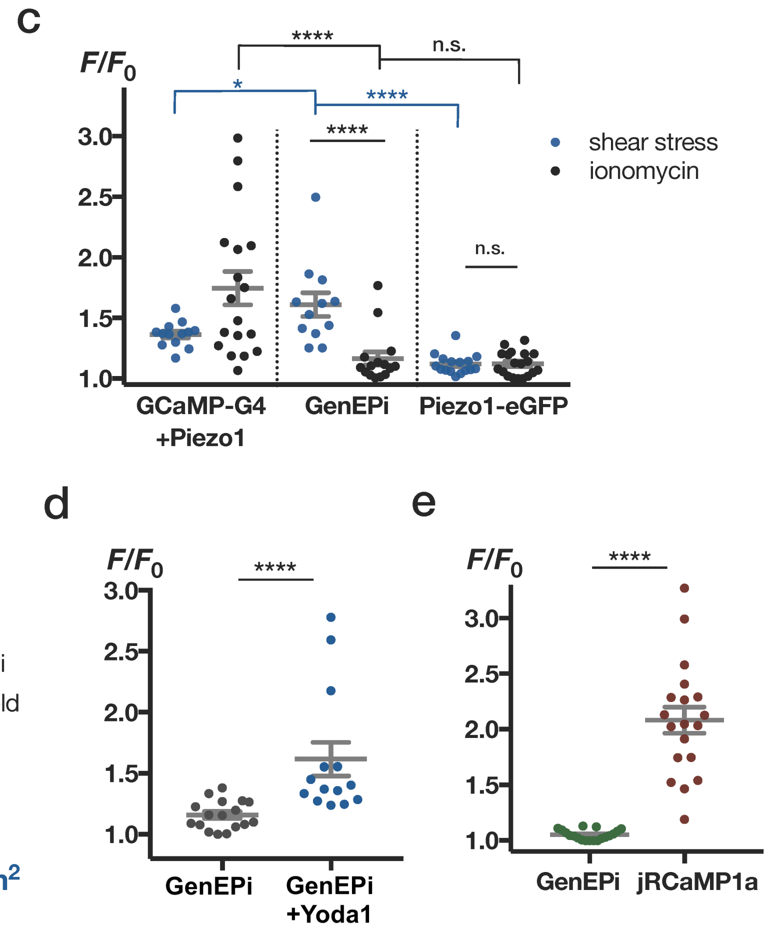

bioRxiv preprint doi: https://doi.org/10.1101/702423; this version posted July 15, 2019. The copyright holder for this preprint (which was not certified by peer review) is the author/funder. It is made available under a CC-BY-NC 4.0 International license.

a

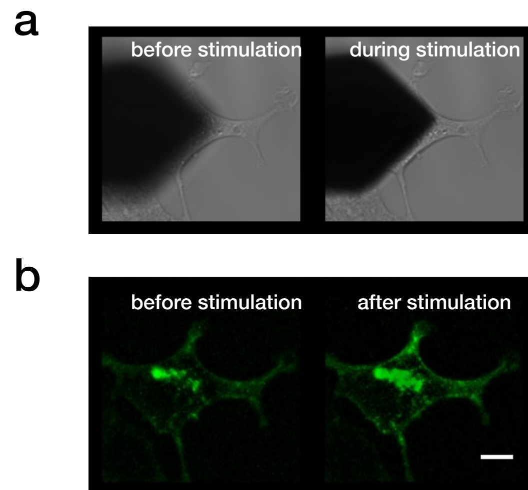

c

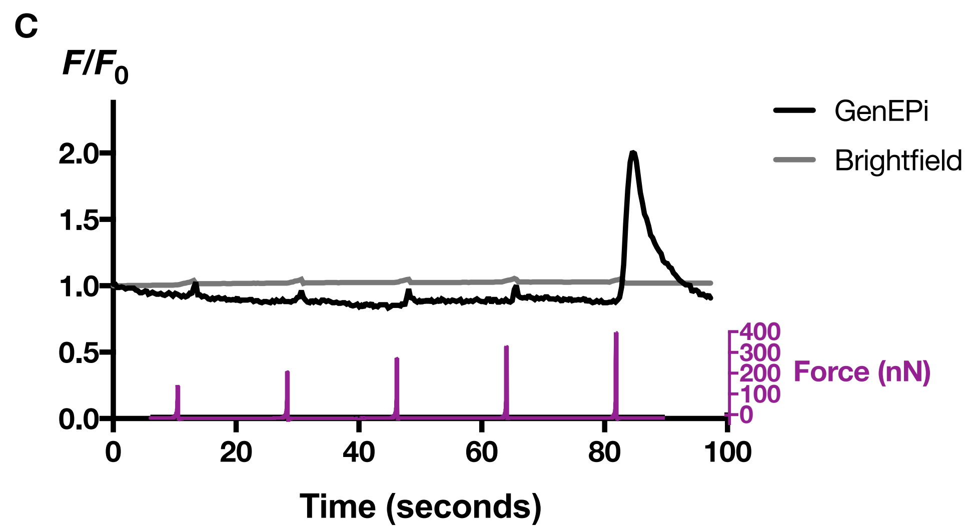

d

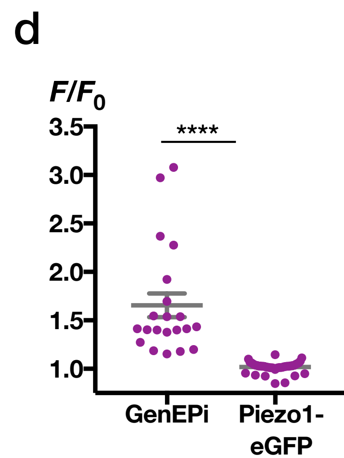

e

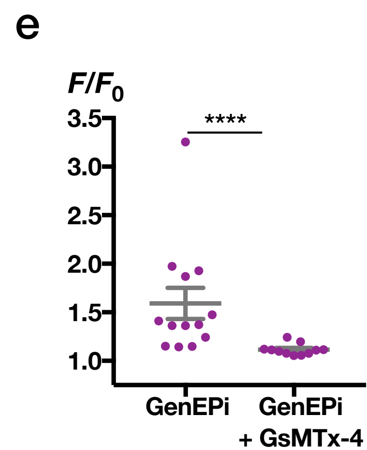

f

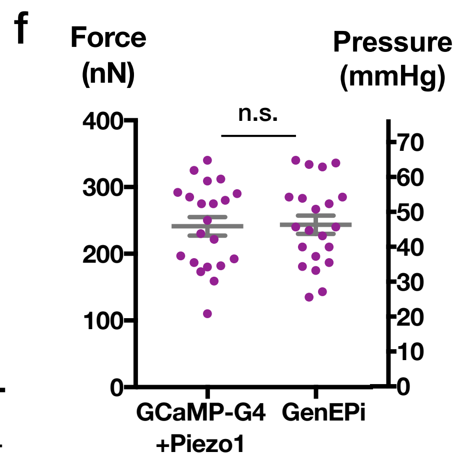

g

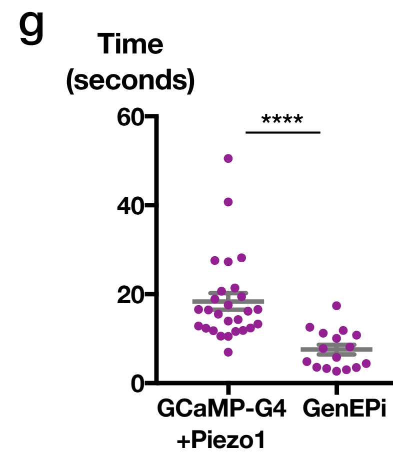

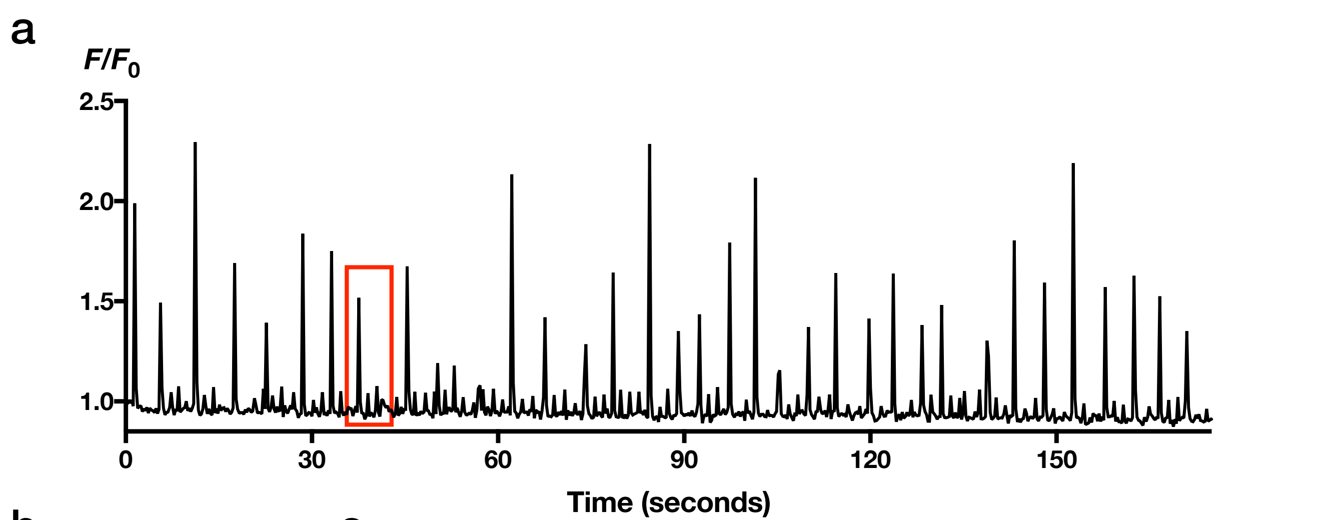
a
F/F0
2.5
2.0
1.5
1.0
0
30
60
90
120
150
Time (seconds)
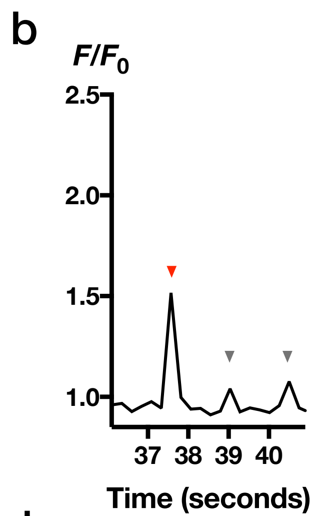
b
F/F0
2.5
2.0
1.5
1.0
37
38
39
40
Time (seconds)
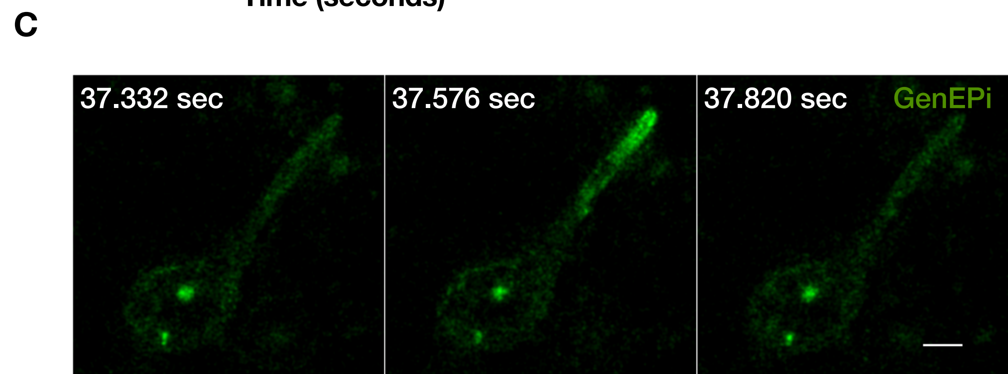
c
37.332 sec
37.576 sec
37.820 sec
GenEPi
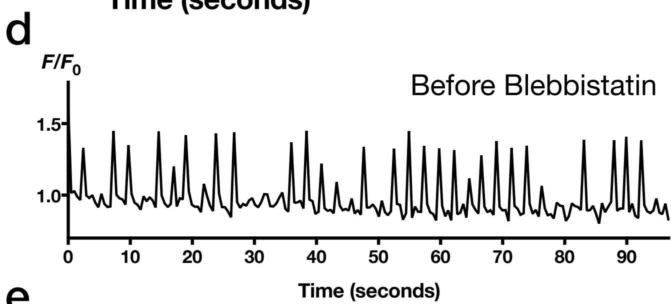
d
F/F0
Before Blebbistatin
1.5
1.0
0
10
20
30
40
50
60
70
80
90
Time (seconds)
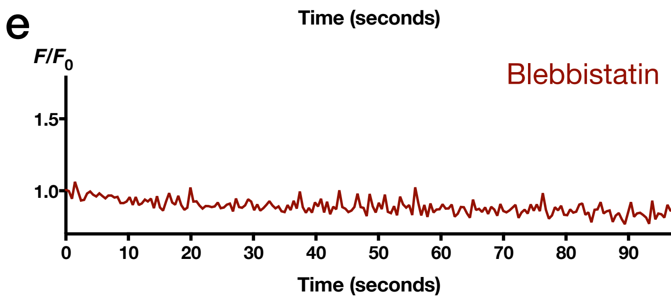
e
F/F0
Blebbistatin
1.5
1.0
0
10
20
30
40
50
60
70
80
90
Time (seconds)
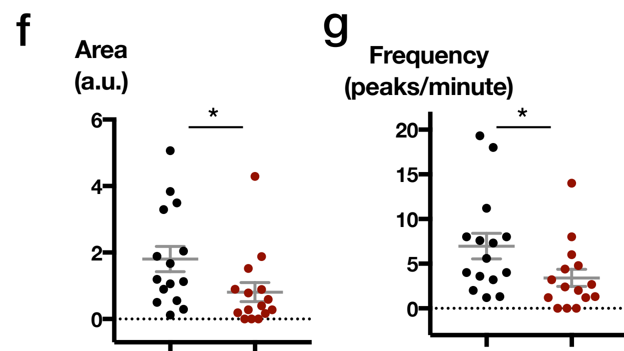
f
Area
(a.u.)
6
4
2
0
*
g
Frequency
(peaks/minute)
20
15
10
5
0
*
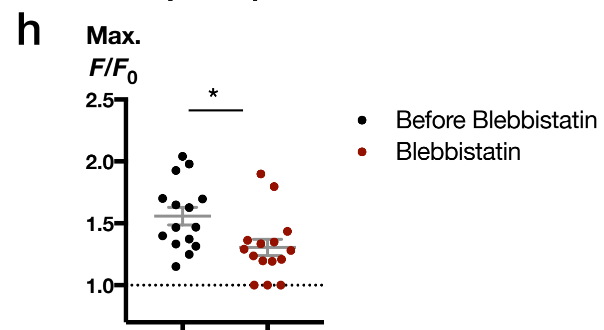
h
Max.
F/F0
2.5
2.0
1.5
1.0
*
Before Blebbistatin
Blebbistatin